Radio Science, Volume 34, Number 2, Pages 427–436, March–April 1999

The Esrange MST radar: A brief introduction and procedure for range validation using balloons

Phillip B. Chilson and Sheila Kirkwood

MRI Atmospheric Research Programme, Swedish Institute of Space Physics, Kiruna, Sweden

Annika Nilsson

Space Engineering Program, Umeå University, Kiruna, Sweden

Abstract. The Esrange VHF radar (ESRAD) is a relatively new mesosphere-stratosphere-troposphere (MST) class radar located in northern Sweden (67.88°N, 21.10°E), about 30 km east of Kiruna. The radar operates continuously and has already been included in several campaigns in which multiple profiling instruments have been used, for example, lidars, radiosondes, and scientific balloons. To intercompare the different measurements, it is essential to have precise height estimates. In this paper we begin by presenting a short technical overview of the radar. Then we describe a radar validation conducted in 1997 during a period when numerous scientific balloons were launched from Esrange. All of these balloons were tracked using one or more of the following techniques: Omega navigational system, Global Positioning System (GPS), or the Esrange C-band tracking radar (ESR). A number of these balloons passed close enough to the ESRAD beam that they could be detected by the MST radar. This unique data set has been used to check the range estimation of ESRAD. Furthermore, the data have been used to make a rough check of the geometry of the formed beam.

1. Introduction

An important contribution to our understanding of the lower to middle atmosphere has come through the use of radars. Most radars used today for the study of the atmosphere are weather radars, which operate in low-elevation horizontal-scan mode. However, there is another variety of atmospheric radar that makes observations using vertical or near-vertical antenna beams. These radars are sometimes called "wind profilers" because of their ability to produce vertical profiles of the three-dimensional wind vector aloft. The name wind profiler, however, is something of a misnomer since the radars can provide much more information than just that pertaining to the wind. For example, they can be used to measure the strength and distribution of atmospheric turbulence, detect the presence of stable atmospheric layers, make precipitation measurements, and even study meteors entering the Earth's atmosphere. See *Atlas* [1990, and references therein] for a comprehensive treatment of atmospheric radars.

Broadly speaking, vertically oriented radars are classified according to their range and/or operating frequency. The three main groups relating to altitude are the boundary layer radars, the stratosphere–troposphere (ST) radars, and the mesosphere–stratosphere–troposphere (MST) radars. The most commonly used frequencies include medium frequency (MF), very high frequency (VHF), and ultra high frequency (UHF). Over the years, we have experienced an ever-growing number of radars falling within these categories distributed across the world. It is not surprising that not only the numbers but also the technological levels of the radars have grown.

There have been many advances in the area of radar studies of the atmosphere regarding both hardware and the interpretation of the resulting data. A review of recent developments is given by *Hocking* [1997a]. One of the advancements is the improved ability of radars to localize scattering targets to a given range interval. That is, the range resolution has improved. Some different means of increasing range resolution include transmit-

Paper number 1998RS900023.
0048-6604/99/1998RS900023$11.00

ting shorter pulses [*Nastrom et al.*, 1998]; implementing FMCW techniques [*Eaton et al.*, 1995]; using a bistatic configuration [*Cho et al.*, 1996]; or taking advantage of interferometry techniques [*Chilson and Schmidt*, 1996].

Of course, as the range resolution for radars improves, it becomes increasingly important to be able to accurately estimate the absolute range to the target. The estimated range to a target is readily calculated from the delay between the time the transmit pulse is sent to when the backscattered radiation is received. The range is simply half the delay time multiplied by the speed of light. However, one must additionally consider several sources of time offsets resulting from built-in hardware delays, type of pulse shaping used, pulse coding, and so forth. If not corrected, errors in the range estimate of hundreds of meters can result. Many radar systems measure these offsets by injecting a signal into the transmitter, which is then fed directly into the receiver. The measured time delay then gives the system time offset. This is not practical, however, for all radars. One example is the large National Astronomy and Ionosphere Center (NAIC) radar located at Arecibo, Puerto Rico. In such cases, alternative means of measuring the time delay must be sought.

We have recently completed a range validation of the new Esrange VHF MST radar (ESRAD) using instrumented balloons together with several different tracking instruments. When the balloons passed through or near the radar beam of ESRAD, they provided an enhancement in the received backscattered signal. From such data we found the range to the balloon relative to the ESRAD system. The position of the balloon was then compared against the range estimates obtained independently from the other tracking instruments. In this paper we begin by giving a brief overview of the technical and operating parameters of ESRAD. Then we describe the execution of the range validation experiment and summarize the results. Finally, we discuss the applicability of these measurements to other MST/ST radars.

2. Technical Description

Since a description of the ESRAD system has not been presented in the literature to date, we begin by giving a brief overview of the technical and operating parameters of the radar. ESRAD is an MST-class VHF radar located in northern Sweden (67.88°N, 21.10°E) above the Arctic circle. It has been in near-continuous operation since June 1996. The transmitter and receiver hardware have been constructed under contract by the Atmospheric Radar Systems Party, Ltd. (ATRAD), of Adelaide, Australia. The antenna installation, the necessary infrastructure, the management of the hardware installation, and the hardware maintenance have been handled by the Swedish Space Corporation (SSC) at Esrange. Scientific data analysis and distribution are conducted by the Swedish Institute of Space Physics (IRF). A summary of the radar's technical parameters are listed in Table 1. Further information can be found on the radar's home page (http://www.irf.se/mst/EsrangeMST.html). For a comparison of ESRAD with other radar facilities see *Hocking* [1997a].

ESRAD operates at a frequency of 52 MHz, corresponding to a wavelength of 5.77 m. The transmitter consists of seventy-two 1-kW solid-state modules that are grouped into twelve 6-kW power blocks. The output from the 12 power blocks is fed uniformly into a phased array antenna as described below. The resulting peak output power is 72 kW, and the maximum duty cycle is 5%. Pulse repetition rates from 100 Hz to 16 kHz and pulse lengths corresponding to range resolutions between 150 m and 3 km are possible. The radar is capable of pulse coding the transmitted signals using both Barker and complementary codes.

The radar has six separate receivers for detection of backscattered signals from the atmosphere. The complex (inphase and quadrature) data samples are recorded using a 12-channel data acquisition unit. The bandwidth of the separate receiving elements is 2 MHz. Using multiple receivers allows postdetection beamsteering and full spectral analysis of the returned signal. The digital processing system has sampling rates corresponding to the range resolutions mentioned above and can process up to 256 ranges per sample and integrate up to 4096 pulse repetitions per sample. Data can be acquired at very high rates, and analog-to-digital (A/D) converters, signal averagers, and temporary data memories are integrated into each channel.

The antenna consists of a 12 × 12 phased array of five-element Yagis, each being approximately 6 m high. The individual elements of the antenna are grouped into 36 "quartets" of four nearest-neighbor Yagis. Three quartets are driven by a single power block. That is, one power block drives 12 Yagi elements. The Yagis themselves are spaced about 4 m apart (corresponding to 0.7 radar wavelengths). The 4 central positions in the array are not filled in order to accommodate a small control hut, which contains the transmitters, receivers, and control computer. Each quartet is separately connected to a patch board in the hut, allowing a large number of different antenna configurations. A diagram of the array layout is shown in

Table 1. Condensed Technical Characteristics

Parameter	Value
Transmitter	
Peak power	72 kW
Duty cycle	up to 5%
Frequency	52 MHz
Pulse repetion rate	20 Hz to 50 kHz
Pulse length	1–50 μs
Coding	complementary[a] and Barker[b]
Antenna	
Number of antennas	140
Antenna spacing	0.7 λ
Antenna area	45 m × 45 m
Beam swinging angles	7°, 14°, 20° in north, south, east, and west directions
Power aperture product	7×10^6 W m^2
Receivers	
Configuration	six separate receivers
Sampling interval	1–20 ms
Filters	250, 500, 1000, and 2000 kHz
Digital Processing	
Number of ranges	1–256
Pre-integrations	1–4096 samples
Standard wind analysis	spaced antenna and Doppler beam swinging

[a]Available code lengths are 2, 4, 8, 10, 16, 32, and 64 bits.
[b]Available code lengths are 2, 3, 4, 5, 7, 11, and 13 bits.

Figure 1. When all the individual elements are driven, the resulting antenna beam has a two-way half-power width of about 5°. The present size of the antenna array results in an estimated power aperture product of better than 7×10^6 W m^2; however, the location of the array permits possible future expansion in all directions.

Basic software for radar control, data acquisition, and computation of wind profiles (running on a PC) was included in the purchase contract from ATRAD. Software for data display, archiving, and further analysis, as well as software for wind estimates derived from meteor echoes, have been implemented as part of a scientific cooperation between the University of Adelaide and IRF Kiruna. All necessary communications and data transfer between the local control system and the processing and control systems located in the Esrange main building utilize an Ethernet connection. A 2-km high-speed link connects the radar site to the main building. The link consists of optical fibers in order to eliminate potential interference problems near the radar transmitters. From Esrange, worldwide communication is performed via Internet.

ESRAD is presently capable of operating in both the spaced antenna (SA) mode [*Briggs*, 1984] and the Doppler beam swinging (DBS) mode [*Woodman and Guillen*, 1974]. The beam swinging and pulse coding enhancements were implemented in April 1997 as part of an upgrade by ATRAD. DBS operation utilizes a hybrid Doppler interferometer mode based on the Adelaide hybrid Doppler interferometer operation as described by *Reid et al.* [1995]. An automated switching system enables multiple sequential measurements with predetermined radar configurations. The radar concept itself in-

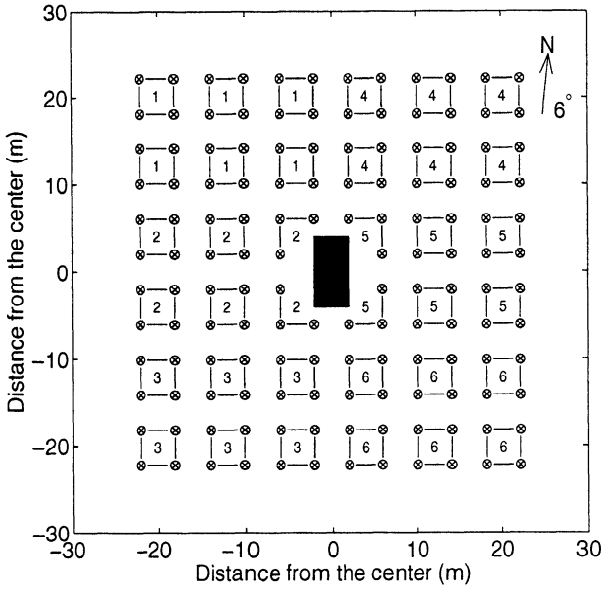

Figure 1. Antenna configuration for the Esrange VHF radar (ESRAD) (6° offset from north). The Yagi antenna elements are aligned in the east-west plane. The location of the radar control hut is shown as the solid rectangle in the center of the figure. The numbers in the individual antenna quartets indicate the receivers to which they were coupled during the experiment

cludes a high level of software control of most parts of ESRAD, resulting in a flexible design which facilitates future expansions.

Another upgrade was completed in February 1998 to allow meteor wind measurements. The analysis uses standard meteor detection techniques. If a meteor is detected by the software, postset beam steering (PSS) [*Kudeki and Woodman*, 1990] is employed to determine the position of the scatterer. The PSS steers the receive beam to a number of different zenith angles and performs a least squares fit to the estimated meteor power for each beam in order to find the direction of maximum power. Once the maximum zenith position has been estimated, the receive beam is steered to this direction and an exponential function is fitted to the amplitude of the meteor event in order to estimate the decay time, and a line is fitted to the phase of the event to estimate the radial velocity of the record.

For the particular experiment discussed here, the radar was operated in a SA mode. Uncoded 2-μs pulses were transmitted, corresponding to a range resolution of 300 m. The pulse repetition frequency was 4096 Hz, and 512 preintegrations were performed before dumping the 320-point time series of complex data to a storage hard disk. The resulting time resolution and dwell time were 0.125 s and 40 s, respectively.

3. Experiment and Analysis

During the validation of the Japanese instrument, ILAS (improved limb atmospheric spectrometer), 23 large scientific balloons in addition to numerous pressure–temperature–humidity sondes (PTU-sondes) were launched from Esrange in the period from February 1 to March 24, 1997. All of these balloons were tracked using one or more of the following techniques: Omega navigational system, Global Positioning System (GPS), or the Esrange C-band (5612-MHz) tracking radar (ESR). A number of these balloons passed close enough to the ESRAD beam that they could be detected by the MST radar. This unique data set has been used to check the range estimation of ESRAD. Furthermore, these data gave us an opportunity to make a rough check of the geometry of the formed beam.

Tracking information for the balloons from the different methods (Omega, GPS, and ESR) was processed by the SSC Esrange. The resulting data sets contain both site-relative and absolute information. Absolute data

Table 2. Balloon Parameters

Date	Separation,[a] m	Separation,[b] m
Feb. 10, 1997	102.1	71.4
Feb. 22, 1997	95.4	74.4
Feb. 26, 1997	95.4	67.4
March 21, 1997	102.1	67.4
March 24, 1997	95.4	67.4

[a]Distance between the balloon and corner reflector.
[b]Distance between the corner reflector and payload.

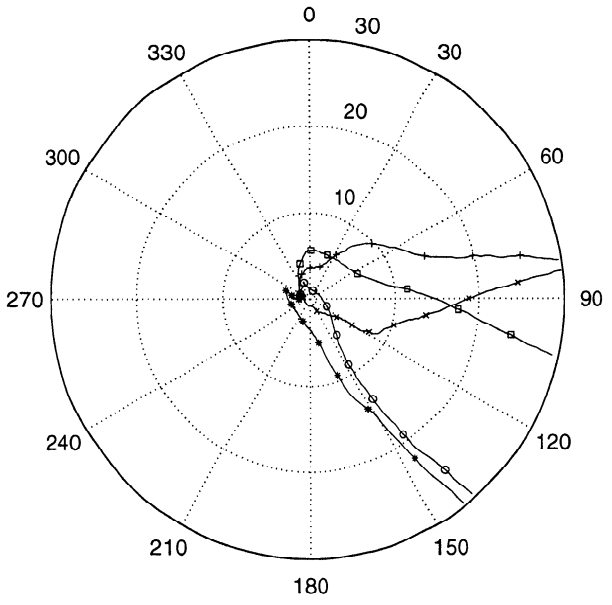

Figure 2. Flight trajectories relative to ESRAD for the different balloons used in this work. Range markers of 10, 20, and 30 km are shown. Symbols are indicated along the flight paths every 5 min.

include the following parameters for the balloon: latitude, longitude, height (above mean sea level), horizontal speed, direction, and ascent rate, together with the time of the observations. We should note here that the height information derived from the GPS sensors used in this experiment is based on pressure measurements. The site-relative data contain the azimuth, elevation, ground range, and slant range of the balloon. We are interested in the position of the balloon relative to ESRAD. Therefore we have calculated the azimuth angle, elevation angle, ground range, and slant range of the balloon with respect to the radar site. Although only the slant range is actually needed to calibrate the range of the radar, it is often useful to know the location of the balloon relative to the radiation pattern of the radar.

4. Results

In this study we have chosen to focus our attention on five particular balloon launches for which the balloon was detected by the ESRAD system. In all of these cases the balloons carried GPS sensors and were tracked using the Esrange tracking radar (ESR). The flight train of the balloons consisted of three components: the balloon, a corner reflector (for the tracking radar), and the scientific payload. Table 2 gives the launch times and the flight train geometry.

The launching site for the balloons lies to the west of ESRAD. During the winter, the prevailing winds near Esrange typically have a strong westerly component. Therefore several balloons launched during the ILAS validation experiment drifted nearly directly over the radar site. The flight trajectories of the five balloons used in this study are shown in Figure 2. The polar plot is drawn relative to the location of ESRAD, where the balloon positions were calculated using the equations given above.

Before looking further into the data, we consider the radiation pattern formed by the ESRAD antenna during the experiment. That is, given the flight trajectory information, we would like to know whether the balloon is expected to be in the main lobe of the radiation pattern, in a sidelobe, or in a null. We have numerically modeled the radiation pattern for the ESRAD system by considering the complex current distribution measured on the

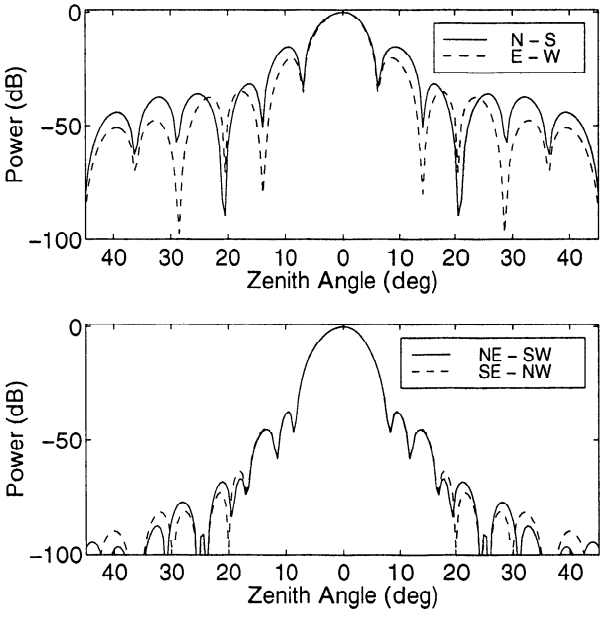

Figure 3. Modeled two-way radiation pattern for the ESRAD antenna assuming transmission from the entire array and reception using a subset of the antenna array linked to a single receiver channel. The antenna elements used in the calculation are those connected to receiver channel 1, as shown in Figure 1.

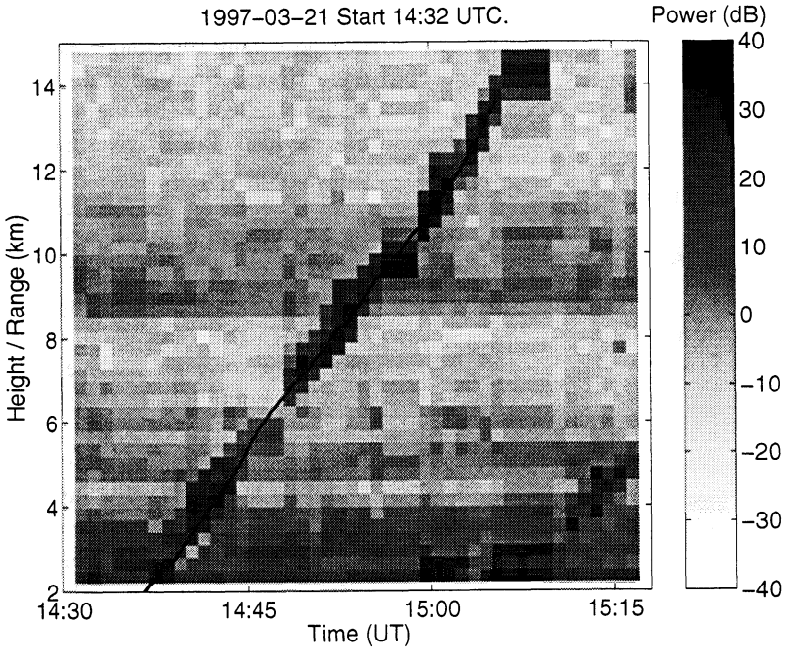

Figure 4. Range-time-intensity plot of radar power showing the signal from a balloon. The solid line represents the trace of the range-time trajectory of the balloon estimated from the tracking radar.

individual antenna elements and then completing a vector sum over the antenna array [e.g., *Czechowsky et al.*, 1984]. When the radar operates in a SA mode, the entire array is used for transmission, but the backscattered signal is received on subsets of the array connected to separate receiver channels, as shown, for example, in Figure 1. The resulting two-way beam pattern when receiver 1 is used for reception is shown in Figure 3. Note that the north-south and east-west slices of the beam pattern contain large sidelobes out to a zenith angle of about 15°. Therefore we can expect the balloons' trajectories shown in Figure 2 to be "within the beam" out to several kilometers from the radar site.

As already mentioned, we have identified several cases in the ESRAD data containing echo signals from balloons. We examine the data from the March 21 balloon launch in detail since for this case the balloon was detected by ESRAD for the longest interval of time. In Figure 4 we present a range-time-intensity plot obtained from ESRAD within the time and height interval in which the balloon was detected. The trace of the balloon is seen as the enhanced trail of signal strength. Note that the labeling on the abscissa depends on the type of backscatter that is detected. The atmospheric signal, having a relatively small backscattering cross section, is only detected by the vertically oriented main beam of the radiation pattern. Therefore the range is equivalent to the height. The balloon, however, is being detected by one or more sidelobes, so here the abscissa corresponds to the range. Overlain on the plot is the actual trace of the range-time trajectory of the balloon obtained from the tracking radar. The range has been converted to be that relative to ESRAD, and the qualitative agreement is good.

Next the signal strength from ESRAD is used to estimate quantitatively the balloon's range from the MST radar site. This is simply done by searching for a local maximum in the backscattered power at approximately the time and range as predicted from the tracking data. A comparison of the range-time estimates for the balloon relative to ESRAD is shown in Figure 5 for the three different tracking techniques. We should mention here that hardware-dependent time delays such as cable lengths and filter delays in the ESRAD system have been measured. Software-dependent corrections to the range estimation, such as pulse shape and coding, are modeled in software. These capabilities were provided by ATRAD.

The data obtained during all balloon launches given in Table 2 have been analyzed using the procedure outlined above. From these data we have calculated averages of the differences between the range-time estimates

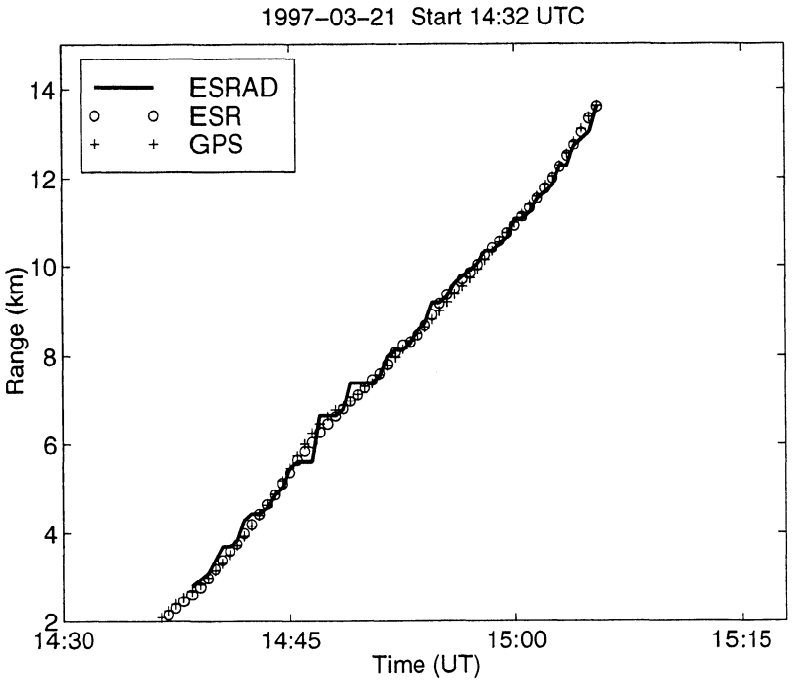

Figure 5. Estimates of the balloon's range-time trajectory based on Global Positioning System (GPS), the Esrange tracking radar (ESR), and the MST radar (ESRAD).

obtained from ESRAD and ESR, ESRAD and GPS, and ESR and GPS. The results are shown in Table 3. In addition to the calculated differences, the standard deviations are listed in parentheses, and the number of data points used are given in the rightmost column. The most accurate of the estimates is expected to come from ESR, and we take these data as the reference. There is only a small differenc between the results from ESRAD and ESR. Although the agreement is quite good, there does appear to be a small offset in the ESRAD range estimate of about 8 m. The offset as estimated using the ESRAD and GPS data is about 35 m.

Finally, we have used these data to obtain a crude check of the modeled radiation pattern for ESRAD shown in Figure 3. The radar equation for a point scatterer is typically given as

$$P_r = P_t \frac{g_t^2 g_r^2 \lambda^2 \sigma_b f_t^2(\theta,\phi) f_r^2(\theta,\phi)}{(4\pi)^3 r^4 l^2}, \qquad (1)$$

where P_r is the received echo power; P_t is the transmit-

Table 3. Comparison of Range Estimates

Date	ESRAD-ESR, m		ESRAD-GPS, m		ESR-GPS, m		Data Points
Feb. 10, 1997	-16.5	(165.3)	-5.0	(152.3)	6.4	(109.9)	23
Feb. 22, 1997	-78.2	(271.3)	-77.7	(359.1)	0.5	(179.4)	31
Feb. 26, 1997	-22.7	(66.3)	-2.1	(88.3)	20.6	(61.9)	10
March 21, 1997	37.4	(164.1)	31.5	(201.1)	-0.4	(138.1)	55
March 24, 1997	54.2	(161.9)	150.0	(169.9)	95.8	(93.3)	43
All days	8.4	(189.8)	34.8	(234.6)	25.2	(134.4)	162

Values in parentheses are the standard deviations.

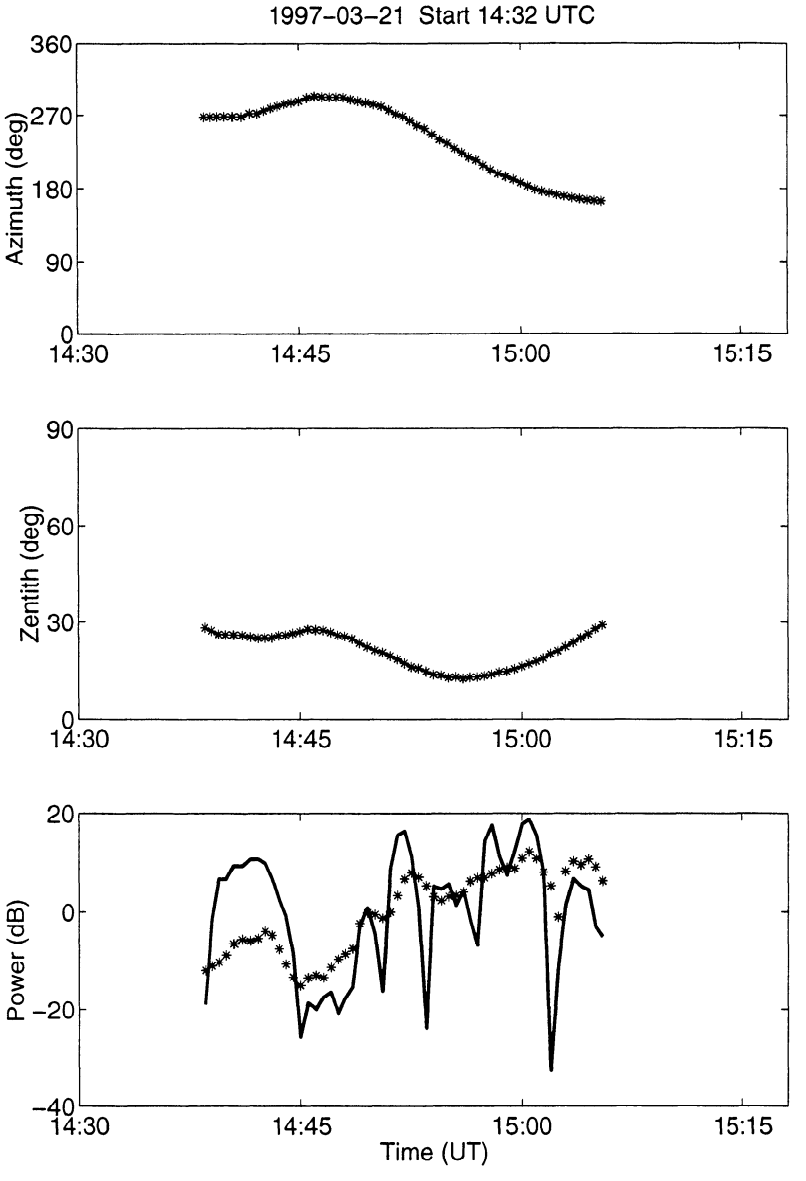

Figure 6. Upper two panels show the position of the balloon as a function of time relative to ESRAD. Lower panel shows relative echo power estimates as a function of time obtained from a model of the two-way antenna pattern (solid line) and range-corrected observations of the echo power (asterisks).

ted power; g_t and g_r are gains of the transmit and receive antennas, respectively; λ is the radar wavelength; σ_b is the backscattering cross section of the target; r is the range; and l^2 is the two-way transmission loss. The radiation patterns of the transmit and receive antennas are given by $f_t^2(\theta, \phi)$ and $f_r^2(\theta, \phi)$, respectively. Therefore, by multiplying the echo power P_r by r^4 and assuming σ^b and l^2 to be constant, we obtain a quantity dependent only on the the product of $f_t^2(\theta, \phi)$ and $f_r^2(\theta, \phi)$. That is the range-normalized power $r^4 P_r$ is directly proportional to the two-way radiation pattern. We have compared the range-normalized power obtained for the March 21 launch data with those expected based on the modeled two-way radiation pattern. The results are shown in the

bottom panel of Figure 6. Note that the values shown in this figure are relative powers. Shown in the upper two panels of Figure 6 are the azimuth and zenith angle of the balloon relative to ESRAD. Although the match is not perfect, many features of the modeled beam pattern are reflected in the observed values.

There are arguably more accurate methods for confirming the modeled radar beam pattern. For example, *Czechowsky et al.* [1984] operated the sounding system (SOUSY) VHF radar in a passive mode while tracking the transit of Cassiopeia A. Although they were able to test the beam-pointing direction with high precision, the strength of the radio source was not sufficient to be detected in the sidelobes of the antenna pattern. Another technique using meteor echoes has been discussed by *Hocking* [1997b]. This technique is not applicable for all radar systems in that it necessitates the capability of making interferometric measurements. We plan to use this method as a future test of the modeled antenna pattern in connection with the new meteor mode capabilities of ESRAD mentioned above.

5. Discussion

We have demonstrated the utility of using instrumented balloons to confirm range estimates obtained for an MST radar. This data set is unique owing to the availability of tracking data from the Omega and GPS systems as well as from the Esrange tracking radar. The excellent agreement between the estimated ranges from ESRAD and those of the tracking radar and GPS should not imply that such a validation is not important. For our case, the good agreement bolsters our confidence in the range values obtained from the ESRAD system. Otherwise, we could have used the results to locate problems in the range determination. Indeed, comparisons similar to those presented above helped to identify an error in the analysis software used to make range corrections for coded signals.

Although we have validated the range information for ESRAD using data from both a C-band tracking radar and GPS receivers, our results indicate the GPS data alone are sufficient for the cross validations discussed here. The accuracy in the comparisons obtained using GPS sensors on balloons is not as good as that from the tracking radar; however, our results show that GPS data are sufficient to check for range estimates accurate to a couple of tens of meters. Since GPS receivers are present in many commercially available radiosondes, the techniques discussed here offer a simple means of validating radar range estimates. We should note that these measurements have been conducted using balloons larger than those typically used during radiosonde launches.

Additionally, we have shown how tracked balloons can be used to provide a rough validation of the modeled beam pattern of an MST radar. The use of balloons in this capacity does not appear to provide an accurate estimate of the exact values of the directional gain. However, the procedure does provide general features of the antenna pattern and in particular can be used to locate the maxima and minima in the beam pattern.

These techniques, although demonstrated on an MST radar, are equally applicable for ST radars as well. We can encourage other radar sites to implement such a validation of the calculated range estimates and antenna patterns.

Acknowledgments. P.B.C. was supported by the Environment and Space Research Institute (MRI) in Kiruna. S.K. and part of ESRAD are financed by the Swedish Natural Science Research Council (NFR). ESRAD is otherwise financed by the Swedish Space Corporation.

References

Atlas, D. (Ed), *Radar in Meteorology*, Am. Meteorol. Soc., Boston, Mass., 1990.

Briggs, B. H., The analysis of spaced sensor records by correlation techniques, in *Handbook for MAP*, edited by R. A. Vincent, vol. 13, pp. 823–833, SCOSTEP Secr., Univ. of Ill., Urbana, 1984.

Chilson, P. B., and G. Schmidt, Implementaion of frequency domain interferometry at the SOUSY VHF radar: First results, *Radio Sci.*, *31*, 263–272, 1996.

Cho, J. Y. N., R. F. Jurgens, and M. A. Slade, High-resolution stratospheric dynamics measurements with the NASA/JPL Goldstone Solar System Radar, *Geophys. Res. Lett.*, *23*, 1909–1912, 1996.

Czechowsky, P., G. Schmidt, and R. Rüster, The mobile SOUSY Doppler radar: Technical design and first results, *Radio Sci.*, *19*, 441–450, 1984.

Eaton, F. D., S. A. McLaughlin, and J. R. Hines, A new frequency-modulated continuous wave radar for studying planetary boundary layer morphology, *Radio Sci.*, *30*, 75–88, 1995.

Hocking, W. K., Recent advances in radar instrumentation and techniques for studies of the mesosphere, stratosphere, and troposphere, *Radio Sci.*, *32*, 2241–2270, 1997a.

Hocking, W. K., System design, signal-processing procedures, and preliminary results for the Canadian (London, Ontario) VHF atmospheric radar, *Radio Sci.*, *32*, 687–706, 1997b.

Kudeki, E., and R. F. Woodman, A poststatistics steering technique for MST radar applicatations, *Radio Sci.*, *25*, 591–594, 1990.

Nastrom, G. D., R. Rüster, and G. Schmidt, The coupling of vertical velocity and signal power observed with the SOUSY VHF Radar, *J. Appl. Meteorol.*, *37*, 114–119, 1998.

Reid, I. M., B. G. W. Vandepeer, S. C. Dillon, and B. M. Fuller, The new Adelaide medium frequency Doppler radar, *Radio Sci.*, *30*, 1177–1189, 1995.

Woodman, R. F., and A. Guillen, Radar observations of winds and turbulence in the stratosphere and mesosphere, *J. Atmos. Sci.*, *31*, 493–505, 1974.

Phillip B. Chilson and Sheila Kirkwood, MRI Atmospheric Research Programme, Swedish Institute of Space Physics, BOX 812, S-981 28 Kiruna, Sweden. (e-mail: phil@irf.se; sheila@irf.se)

Annika Nilsson, Space Engineering Program, Umeå University, BOX 812, S-981 28 Kiruna, Sweden.

(Received May 5, 1998; revised August 21, 1998; accepted October 26, 1998.)